CrystEngComm

PAPER

View Article Online
View Journal | View Issue

Cite this: *CrystEngComm*, 2016, **18**, 309

Synthesis of $ZnWO_4/CdWO_4$ core–shell structured nanorods formed by an oriented attachment mechanism with enhanced photocatalytic performances

Di Li,*[a] Juanqin Xue[a] and Xiaojuan Bai[b]

Received 19th September 2015,
Accepted 26th November 2015

DOI: 10.1039/c5ce01858g

www.rsc.org/crystengcomm

$ZnWO_4/CdWO_4$ core–shell structured nanorods have been synthesized using a simple refluxing method under mild conditions in which the crystallization event of $ZnWO_4$ happened on the backbone of $CdWO_4$ single crystalline nanorods in a ligand-free system. A $CdWO_4$ nanorod-directed oriented attachment mechanism was clearly observed for the formation of the $ZnWO_4/CdWO_4$ core–shell structured nanorods. The size of the $ZnWO_4$ could be tuned by changing the molar ratio of the Zn source and the Cd source. The photocatalytic activity of the $ZnWO_4/CdWO_4$ core–shell structured nanorods was much better than for $CdWO_4$. The enhancement in photocatalytic performance was demonstrated to be due to the match in lattice and energy levels between the $ZnWO_4$ and $CdWO_4$. This match facilitated the separation and transfer of photogenerated e^-/h^+ pairs at the heterojunction interfaces and might be important for other heterostructured materials. Kinetic studies using radical scavenger technologies suggested that photogenerated holes were the dominant photooxidants.

1. Introduction

The growth mechanism involving mostly oriented particle aggregation,[1–4] which was termed conceptually as 'oriented attachment' by Penn and Banfield *et al.*,[5–9] has emerged as highlighted by Alivisatos.[10] In this mechanism, the bigger particles are grown from small primary nanoparticles through an orientated attachment process, in which adjacent nanoparticles that share a common crystallographic orientation are self-assembled by docking at a planar interface.[6]

Metal tungstates and molybdates, as a family of multicomponent metal oxide compounds, have been studied extensively due to their interesting structures and intriguing physical–chemical properties, as well as their wide range of applications in photoluminescence,[11] magnetic materials,[12] electrochemistry[13] and photocatalysis.[14–20] $ZnWO_4$ and $CdWO_4$ have the potential to produce a highly efficient photocatalytic material.[21–28] Therefore, there was a need to investigate the photocatalytic activity of a $ZnWO_4/CdWO_4$ core–shell structured photocatalyst.

In this paper, we have described the oriented attachment mechanism in which $CdWO_4$ nanorods obviously act as an epitaxial 'substrate' and guide a $ZnWO_4$ aggregation process for the formation of $CdWO_4$ nanorod based core–shell structures. The $ZnWO_4/CdWO_4$ core–shell structured nanorods were controllably synthesized using a facile refluxing method under mild conditions. The $CdWO_4$ nanorods form the backbone of the material, and the $ZnWO_4$ size could be tuned by changing the molar ratio of the Zn source and the Cd source. In addition, the photocatalytic activity and degradation mechanism of the $ZnWO_4/CdWO_4$ core–shell structured nanorods in the degradation of methylene blue (MB) under ultraviolet light irradiation were investigated in detail.

2. Experimental section

2.1. Preparation of $CdWO_4$ nanorods and $ZnWO_4/CdWO_4$ core–shell structured nanorods

$CdWO_4$ nanorods were synthesized in a 50 mL capacity Teflon-lined stainless steel autoclave, which was used in a digital-type temperature controlled oven. The detailed synthetic procedure for $CdWO_4$ nanorods has been described previously.[28] The synthesis of the hierarchical $ZnWO_4/CdWO_4$ core–shell structured nanorods was performed in a flask under mild magnetic stirring for different periods. Typically, the $CdWO_4$ nanorods were dispersed in 100 mL of water. Then, $Zn(NO_3)_2$ and the same amount of Na_2WO_4 were added to the mother solution discontinuously. The solution was refluxed for 24 h. Finally, the precipitate was washed with

[a] *School of Metallurgical Engineering, Xi'an University of Architecture and Technology, Xi'an, 710055, China. E-mail: lidi80315@gmail.com*
[b] *Academy of State Administration of Grain P.R.C, No. 11 Baiwanzhuang Avenue, Xicheng District, Beijing 100037, China*

distilled water three times and dried for further characterization. The $ZnWO_4$ size could be tuned by changing the molar ratio of the Zn source and the Cd source.

2.2. Characterizations

X-ray diffraction (XRD) experiments were carried out using a Rigaku D/MAX-2500 diffractometer with Cu Kα radiation. The pH value was measured using an OHAUS STARTER 2100/3C Pro-B pH meter. The sizes and morphologies of the $CdWO_4$ and $ZnWO_4/CdWO_4$ core–shell structured nanorods were characterized with the aid of a JEOL JEM-2100F transmission electron microscope (TEM) and FEI Tecnai G2 F20 field transmittance electron microscope. The Brunauer–Emmett–Teller (BET) surface area was measured by ASAP 2020. X-ray photoelectron spectroscopy (XPS) measurements were performed using a Kratos AXIS ULTRA DLD. The transient photoluminescence measurements were carried out using a steady state and time-resolved fluorescence/phosphorescence spectrometer (FLSP920, Edinburgh Instruments Ltd.). EPR measurements of radicals spin-trapped by spin-trap reagent 5,50-dimethyl-1-pirroline-*N*-oxide (DMPO) (purchased from Sigma Chemical Co.) were carried out at room temperature using a JEOL ES-ED3X spectrometer equipped with a high-pressure mercury lamp as the irradiation source. To minimize experimental errors, the same type of quartz capillary tube was used for all EPR measurements. The EPR spectrometer was coupled to a computer for data acquisition and instrument control. Magnetic parameters of the detected radicals were obtained from direct measurements of the magnetic field and microwave frequency.

2.3. Photocatalytic oxidative degradation

The photocatalytic activities of the $CdWO_4$ and $ZnWO_4/CdWO_4$ core–shell structured nanorods were evaluated using the MB decomposition under ultraviolet irradiation. Ultraviolet (UV) light was obtained from a 15 W Hg lamp (λ = 254 nm, Cnlight, Feshan) and the average light intensity was 600 μW cm^{-2}. The radiant flux was measured using a power meter (Beijing Normal University, Beijing). The photocatalytic degradation of MB in the aqueous solutions was studied using $CdWO_4$ or $ZnWO_4/CdWO_4$ core–shell structured nanorods as the photocatalysts under room temperature and normal atmosphere pressure. The $CdWO_4$ (50 mg) or $ZnWO_4/CdWO_4$ core–shell structured nanorods (50 mg) and 100 mL of the MB (2×10^{-5} M) aqueous solution were added into the reactor, and then stirred with a magnetic stirrer prior to irradiation with the Hg lamp at room temperature. After the reaction, the sample solution was put into a centrifuge to remove $CdWO_4$ particles from the solution. The solution that was obtained this way was extracted into a quartz cell. The absorbance of the solution was measured using the quartz cells every 5 min.

3. Results and discussion

3.1. Characterization of $ZnWO_4/CdWO_4$ core–shell structured nanorods

To determine the phase structures of the products, X-ray diffraction (XRD) measurements were conducted. The backbone material, $CdWO_4$ nanorods ($CdWO_4$: JCPDS card no. 87-1114), was identified by the XRD patterns shown in Fig. 1a. Because $CdWO_4$ (no. 87-1114: a = 5.029 Å, b = 5.86 Å, c = 5.071 Å, α = 90°, β = 91.5°, γ = 90°) had a similar crystal lattice parameter as $ZnWO_4$ (no.88-0251: a = 4.693 Å, b = 5.721 Å, c = 4.928 Å, α = 90°, β = 90.63°, γ = 90°), lattice matching between $CdWO_4$ and $ZnWO_4$ could exist.

Fig. 2a–d shows the TEM images of the $CdWO_4$ nanorods and obtained $ZnWO_4/CdWO_4$ core–shell structured nanorods with different initial molar ratios of the Zn source and the Cd source. In Fig. 2a, pure $CdWO_4$ nanorods with lengths of 150–200 nm and diameters of 30–50 nm were used as the backbone material. The core–shell structure of the $ZnWO_4/CdWO_4$ sample is shown in Fig. 2b–d. Fig. 2b indicates that $ZnWO_4$ tends to attach on the backbone of the $CdWO_4$ nanorods. As shown in Fig. 2b–d, the size of the $ZnWO_4$ would increase with an increasing molar ratio of the Zn source and the Cd source. When the molar ratio of the Zn source and the Cd source was 1 : 10, most of the as-obtained nanorods had a smooth surface (Fig. 2b). However, when the molar ratio increased from 1 : 10 to 2 : 10 and 4 : 10, respectively, the surfaces of the nanorods became rougher and rougher (Fig. 2c and d), indicating that the size of the $ZnWO_4$ shell became thicker. The microstructures of the $ZnWO_4/CdWO_4$ core–shell structured nanorods were then investigated using high-resolution TEM (HRTEM). The HRTEM image (Fig. 2e) shows that the interplanar spacing of the nanorod was about 3.8 Å, which coordinates with the XRD peak for the [111] plane (2θ = 29.559°). The selected area fast Fourier transform (FFT) pattern, as shown in Fig. 2f, confirmed that the nanorods were single crystalline. In order to further confirm the chemical composition and elemental distribution, scanning transmission electron microscope (STEM) studies were performed. As displayed in Fig. 2g–j, the Cd, W and Zn elements were distributed in the nanorods. The Cd atoms were distributed in the 'core' of the nanorods; the Zn atoms

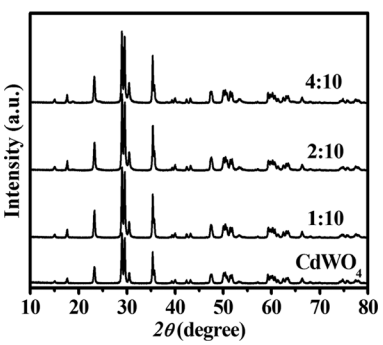

Fig. 1 XRD patterns of $CdWO_4$ nanorods and $ZnWO_4/CdWO_4$ core–shell structured nanorods.

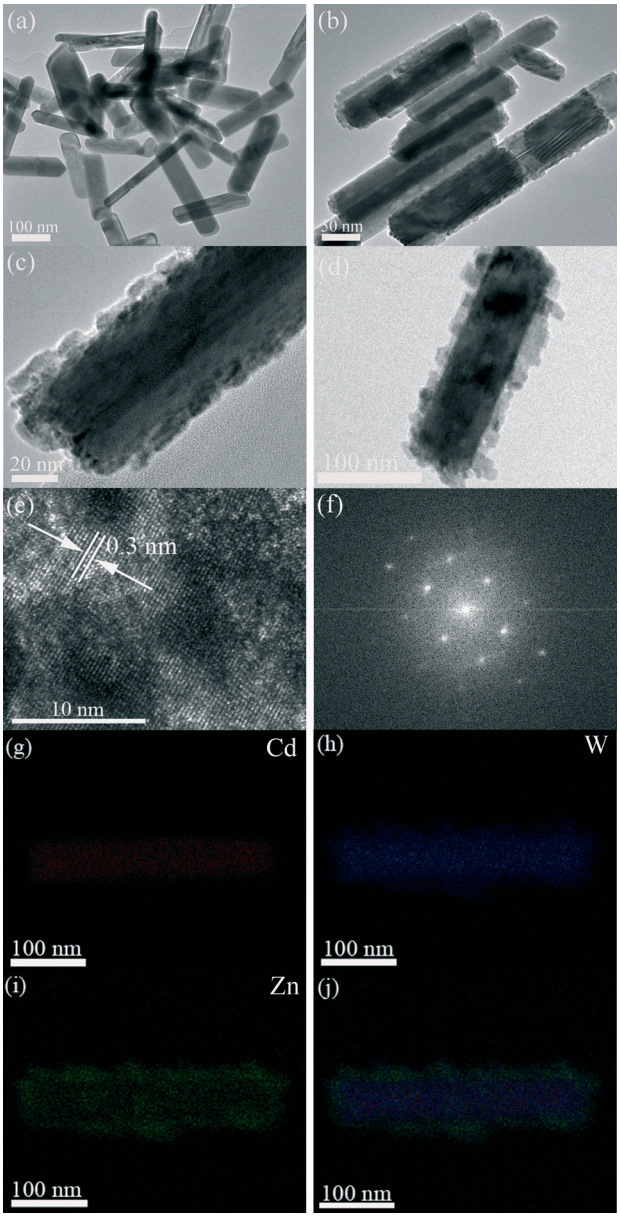

Fig. 2 (a) TEM image of $CdWO_4$ nanorods; (b)–(d) TEM images of the $ZnWO_4/CdWO_4$ core–shell structured nanorods obtained when the molar ratio of Cd source/Zn source in the reaction system was kept as 1 : 10, 2 : 10 and 4 : 10, respectively; (e) HRTEM image of the $ZnWO_4/CdWO_4$ core–shell structured nanorods; (f) the selected area FFT pattern of the $ZnWO_4/CdWO_4$ core–shell structured nanorods in (e); (g), (h) and (i) Cd, W and Zn elemental maps, respectively; (j) Cd, W and Zn elemental map together.

were distributed at the surface of nanorods (Fig. 2i); whereas the W atoms were spread all over the nanorods, indicating that the shell was mainly made of $ZnWO_4$ and the core–shell structures were a mixture of $ZnWO_4$ and $CdWO_4$, which agrees well with the results of the XRD analysis.

XPS was used to analyze the oxidation state and to further study the interaction of $CdWO_4$ covered with the $ZnWO_4$. The XPS spectra of Cd 3d for pure $CdWO_4$ and $ZnWO_4/CdWO_4$ (the molar ratio of the Zn source and the Cd source was 2 : 10), as well as the Zn 2p spectra for $ZnWO_4/CdWO_4$ are shown in Fig. 3a and b. The binding energy of the Cd 3d of $ZnWO_4/CdWO_4$ exhibited an obvious shift as compared to that for pure $CdWO_4$ (Fig. 3a). These results showed that there was an intense interface interaction between the Cd and $ZnWO_4$, not a simply physical adsorption. This interaction was essential to transfer carriers and enhance photocatalytic activity. The peak with binding energy for Zn 2p was detectable (Fig. 3b), indicating the existence of $ZnWO_4$, which was in good agreement with the results from the map analysis.

3.2. Formation process of $ZnWO_4/CdWO_4$ core–shell structured nanorods

The refluxing of a fresh mixture of $Zn(NO_3)_2$ and Na_2WO_4 solutions in the presence of a suitable amount of single-crystal $CdWO_4$ nanorods for different reaction time produced $ZnWO_4/CdWO_4$ core–shell structured nanorods with typical shapes as shown in Fig. 4a and b. Fig. 4a indicates that $ZnWO_4$ tends to attach on the backbone of the $CdWO_4$ nanorods. As the reaction continued, the $ZnWO_4$ grew (Fig. 4b).

3.3. $ZnWO_4/CdWO_4$ core–shell structured nanorods growth mechanism

The growth mechanism of 'oriented attachment' was proposed to demonstrate the complicated nano-architecture process. The oriented attachment mechanism described the

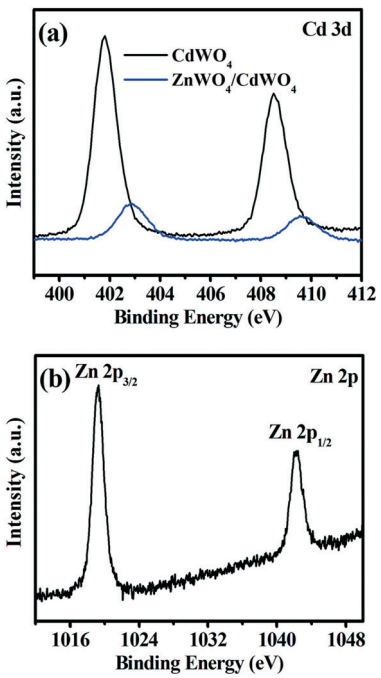

Fig. 3 XPS spectra for: (a) the Cd 3d peak of pure $CdWO_4$ and $ZnWO_4/CdWO_4$ core–shell structured nanorods, (b) the Zn 2p peak of $ZnWO_4/CdWO_4$ core–shell structured nanorods.

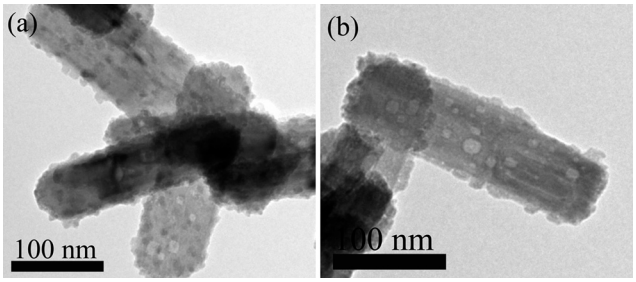

Fig. 4 Typical TEM images of the samples which were taken out after adding $Zn(NO_3)_2$ and Na_2WO_4 to a 100 mL solution containing 3 mmol of $CdWO_4$ nanorods and refluxing the mixture for different periods of time when the molar ratio of the Cd source/Zn source in the reaction system was kept as 2 : 10: (a) refluxing for 6 h and (b) refluxing for 18 h.

spontaneous self-organization of adjacent particles, so that they shared a common crystallographic orientation, followed by the joining of these particles at a planar interface.[13] This process is particularly relevant in the nanocrystalline regime, where bonding between particles reduces overall energy by removing surface energy associated with unsatisfied bonds.[29] In the reaction, $CdWO_4$ nanorods were used as the 'substrate', which can guide the $ZnWO_4$ self-assembling growth in aqueous solution without surfactant and stabilizers. Then the 'oriented attachment' could guide the $ZnWO_4$ oriented growth. As shown in Scheme 1, a supersaturated solution containing plenty of $ZnWO_4$ small crystals was formed by adding the Zn resource. Because of the high surface energy and thermodynamic instability, $ZnWO_4$ could attach to the surface of the $CdWO_4$ to decrease the surface energy. The crystallographic orientation of the particles with respect to each other was determined by the minimization of the highest surface energy. Therefore, with a matching lattice, the lattice fringes' orientation and crystal growth direction were uniform to some extent. The 'substrate', $CdWO_4$, had similar lattice parameters and could control $ZnWO_4$ to form $ZnWO_4/CdWO_4$ core–shell structured nanorods.

3.4. Photocatalytic properties of the $ZnWO_4/CdWO_4$ core–shell structured nanorods

The photoactivity of the $ZnWO_4/CdWO_4$ core–shell structured nanorods was evaluated using the degradation of methylene blue, a hazardous dye as well as a common model to test photodegradation capability.[30–32] To further depict the photocatalytic reaction, the photocatalytic degradation process was also fitted to pseudo-first-order kinetics, and the value of the rate constant k was equal to the corresponding slope of the fitting line, as shown in Fig. 5. The first-order linear relationship was revealed by the plots of the $\ln(C/C_0)$ *vs.* irradiation time (t), where C is the concentration of MB at the irradiation time t and C_0 is the concentration in the adsorption equilibrium of the photocatalysts before irradiation. *Via* the first order linear fit, the determined reaction-rate constants k were 0.02761, 0.04706, 0.06092 and 0.04696 min^{-1}, respectively, for the $CdWO_4$ nanorods and $ZnWO_4/CdWO_4$ core–shell structured nanorods with molar ratios of the Zn source and the Cd source of 1 : 10, 2 : 10 and 4 : 10. The photocatalytic rate constant was obviously enhanced with increasing the $ZnWO_4$ content. When the molar ratio of the Zn source and the Cd source was 2 : 10 (ZC-2), it exhibited the highest photocatalytic activity. The apparent rate constant k was 0.06092 min^{-1}, which was more than twice as high as for the $CdWO_4$ nanorods. However, as the proportion of $ZnWO_4$ further increases, the degradation rate decreases gradually though it remained higher than that of $CdWO_4$. This change in the UV activity of the $ZnWO_4/CdWO_4$ core–shell structured nanorod samples might be attributed to the excitation of $CdWO_4$. Although $ZnWO_4$ was beneficial for charge transfer at heterojunction interfaces, it would shield UV light off of $CdWO_4$. Therefore, due to the demands of both the charge transfer and light harvesting, our photocatalytic activity first increased and then decreased with the increasing amount of $ZnWO_4$, which resulted in the best photocatalytic activity of ZC-2. Additionally, the surface areas of the $CdWO_4$ nanorods and $ZnWO_4/CdWO_4$ core–shell structured nanorods were similar (Table 1), so the surface area had no effect on the photocatalytic activity.

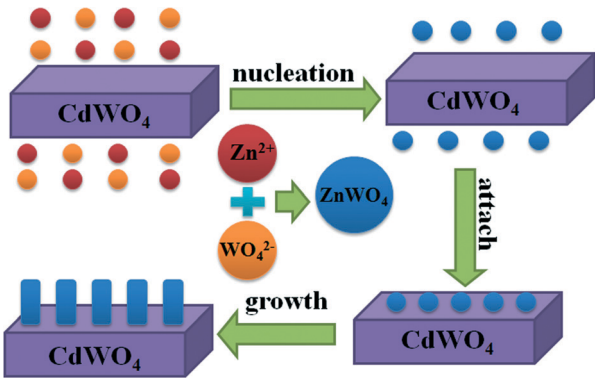

Scheme 1 Schematic drawing illustrating the formation process of the $ZnWO_4/CdWO_4$ core–shell structured nanorods.

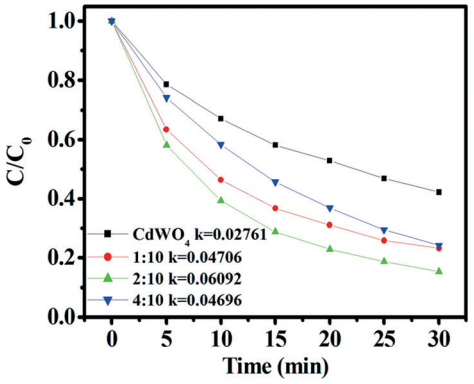

Fig. 5 First-order plots for the photocatalytic degradation of MB using $CdWO_4$ nanorods and $ZnWO_4/CdWO_4$ core–shell structured nanorods.

Table 1 The BET results of $CdWO_4$ nanorods and $ZnWO_4/CdWO_4$ core–shell structured nanorods

Sample	$CdWO_4$	1 : 10	2 : 10	4 : 10
BET surface area ($m^2\ g^{-1}$)	10.3789	8.2022	9.5981	14.5013

It was important to detect the main oxidative species in the photocatalytic process to reveal the photocatalytic mechanism. The main oxidative species in the photocatalytic process could be detected through trapping experiments of radicals and holes using *tert*-butanol (hydroxyl radical scavenger)[33,34] and citric acid (hole scavenger),[35] respectively. As shown in Fig. 6, the addition of a scavenger of radicals (*tert*-butanol) only caused a smaller change in the photodegradation of MB, indicating that the free hydroxyl radicals were not the main active oxygen species in the photocatalytic process. On the contrary, the photocatalytic activity of $ZnWO_4/CdWO_4$ could be greatly suppressed by the addition of a scavenger for holes (citric acid). This result suggested that the photogenerated holes were the main oxidative species of the $ZnWO_4/CdWO_4$ system.

Although the photogenerated holes were the main oxidative species, the reaction-rate decreased more than one fourth after adding *tert*-butyl alcohol (hydroxyl radical scavenger). This meant that the hydroxyl radicals played a part in the photooxidation of MB. EPR spectroscopy was an especially suitable technique for the detection of the photogenerated radicals, which act as intermediates in the photocatalytic processes. Here, the ZC-2 nanorods in water were used to investigate the EPR signal at room temperature under the irradiation of a high-pressure mercury lamp. The results of the EPR signals from the ZC-2 nanorods in water are shown in Fig. 7. No ESR signals were observed when the reaction was performed in the dark in the presence of the catalysts. Under UV irradiation, the characteristic peaks of the $O_2^{\cdot-}$ could be observed after a 1 min illumination period; the superoxide radical anion tends to convert to $OH^{\cdot}$ with the irradiation time increasing.[36,37] The intensity of the $OH^{\cdot}$ further increased with 3 min of irradiation.

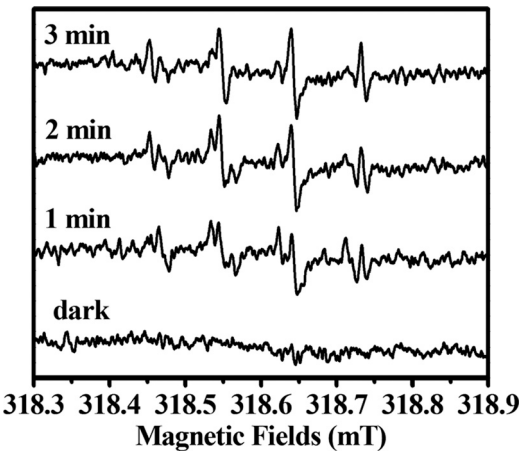

Fig. 7 EPR spectra of the ZC-2 nanorods under UV light irradiation (DMPO as the radical trapper).

N-Demethylation of MB was observed by Mohammad and Morrison[38] during "photodynamic therapy" studies using visible light irradiation ($\lambda > 520$ nm). *N*-Dealkylation of dyes containing auxochromic alkylamine groups played an important role in photocatalytic degradation. The colour of MB solutions became less intense (hypsochromic effect) when all or part of the auxochromic groups (methyl or methylamine) degraded. Fig. 8 shows that the spectral band at 664 nm blue-shifted during the course of the photodegradation. As weak electron donor substituents, methyl groups could facilitate an attack on MB by electrophilic species ($OH^{\cdot}$ or hole) in the demethylation process; this was also likely to be a major step in the photocatalytic oxidative degradation of MB.[39] Examination of the spectral variations in Fig. 8 suggested that MB was *N*-demethylated in a stepwise manner (methyl groups were removed one at a time as confirmed by the gradual peak wavelength shifts toward the blue region), with cleavage of the MB chromophore ring structure occurring concomitantly. *N*-Demethylation, deamination and oxidative degradation took place during the photocatalyzed degradation of MB.[39] Mixtures of *N*-demethylated intermediates

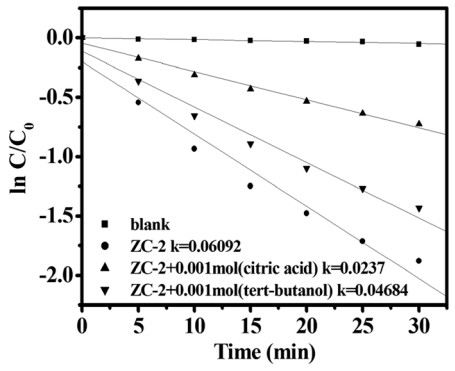

Fig. 6 Effects of *tert*-butyl alcohol and citric acid addition on the photocatalytic degradation of MB in solutions of ZC-2.

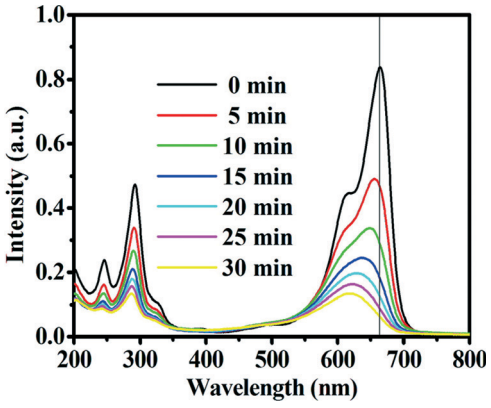

Fig. 8 The UV-vis spectral changes of MB (ZC-2: 0.5 g L^{-1}; MB: 2×10^{-5} M).

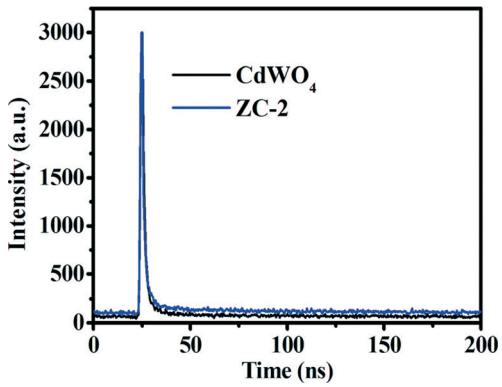

Fig. 9 Time-resolved transient photoluminescence decays of $CdWO_4$ and ZC-2.

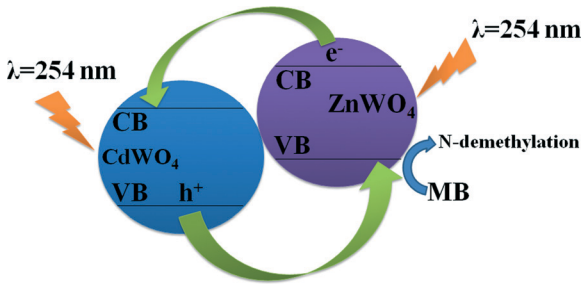

Scheme 2 Schematic drawing illustrating the mechanism of charge separation and photocatalytic activity over the $ZnWO_4/CdWO_4$ core–shell structured nanorods under ultraviolet light irradiation.

yielded spectra with broad absorption bands in the visible range.

The above results showed that the coating of $ZnWO_4$ could enhance the UV activity of $CdWO_4$. As was well known, this might be due to the high separation and transfer of photogenerated electron–hole pairs at the heterojunction interfaces. Fig. 9 shows time-resolved transient photoluminescence decays of $CdWO_4$ and the sample ZC-2. The photoluminescence lifetimes of the $CdWO_4$ and $ZnWO_4/CdWO_4$ core–shell structured nanorods were in the order of nanoseconds, and the photoluminescence lifetime of ZC-2 was higher than that of $CdWO_4$: ZC-2 (28.19 ns) > $CdWO_4$ (11.34 ns). A longer photoluminescence lifetime meant a lower recombination rate of the electron–hole pairs, and thus a higher photocatalytic activity.[40]

This high separation efficiency may be due to the energy level match between $ZnWO_4$ and $CdWO_4$. Scheme 2 shows the schematic for e^-/h^+ separation and transportation at the $ZnWO_4/CdWO_4$ core–shell structured nanorod interface. Both the $ZnWO_4$ and $CdWO_4$ can absorb UV light to produce photogenerated electron–hole pairs. Since the valence band (VB) position of the $ZnWO_4$ (+2.9 eV) is higher than the VB of $CdWO_4$ (+3.43 eV),[41,42] the photogenerated holes on the VB of $CdWO_4$ can directly transfer to the VB of $ZnWO_4$. On the contrary, the conduction band (CB) position for the $ZnWO_4$ (−0.8 eV) is higher than that of $CdWO_4$ (+0.13 eV). So the excited-state electrons from the CB of $ZnWO_4$ start to diffuse into the CB of $CdWO_4$. Therefore, an effective charge separation was achieved, resulting in an increased photocatalytic activity.

4. Conclusions

In summary, $ZnWO_4/CdWO_4$ core–shell structured nanorods could be synthesized by a facile refluxing method under mild conditions in which the crystallization event of $ZnWO_4$ occurred on the backbone of $CdWO_4$ nanorods. The size of the $ZnWO_4$ could be tuned by changing the molar ratio of the raw materials. The enhancement of the UV light performance was induced by the high separation efficiency of the photoinduced electron–hole pairs. This high separation efficiency might be due to the heterojunction interfaces induced by the lattice and the energy match. The $ZnWO_4/CdWO_4$ core–shell structured nanorods described in this paper might have potential applications in photocatalytic decomposition of MB.

Acknowledgements

This work was supported by Chinese National Science Foundation (21301135).

Notes and references

1 J. K. Bailey, C. J. Brinker and M. L. Mecartney, *J. Colloid Interface Sci.*, 1993, **157**, 1.
2 M. Ocaña, M. P. Morales and C. J. Serna, *J. Colloid Interface Sci.*, 1995, **171**, 85.
3 V. Privman, D. V. Goia, J. Park and E. Matijević, *J. Colloid Interface Sci.*, 1999, **213**, 36.
4 A. Chemseddine and T. Moritz, *Eur. J. Inorg. Chem.*, 1999, 235.
5 R. Lee Penn and J. F. Banfield, *Geochim. Cosmochim. Acta*, 1999, **63**, 1549.
6 R. Lee Penn and J. F. Banfield, *Science*, 1998, **281**, 969.
7 J. F. Banfield, S. A. Welch, H. Zhang, T. T. Ebert and R. Lee Penn, *Science*, 2000, **289**, 751.
8 R. Lee Penn, G. Oskam, T. J. Strathmann, P. C. Searson, A. T. Stone and D. R. Veblen, *J. Phys. Chem. B*, 2001, **105**, 2177.
9 R. L. Penn, A. T. Stone and D. R. Veblen, *J. Phys. Chem. B*, 2001, **105**, 4690.
10 A. P. Alivisatos, *Science*, 2000, **289**, 736.
11 B. Liu, S.-H. Yu, L. Li, F. Zhang, Q. Zhang, M. Yoshimura and P. Shen, *J. Phys. Chem. B*, 2004, **108**, 2788.
12 Q. Zhang, X. Chen, Y. Zhou, G. Zhang and S.-H. Yu, *J. Phys. Chem. C*, 2007, **111**, 3927.
13 L. Mai, F. Yang, Y. Zhao, X. Xu, L. Xu and Y. Luo, *Nat. Commun.*, 2011, **2**, 381.
14 L. Zhou, W. Wang, H. Xu and S. Sun, *Cryst. Growth Des.*, 2008, **8**, 3595.
15 S. Song, Y. Zhang, Y. Xing, C. Wang, J. Feng, W. Shi, G. Zheng and H. Zhang, *Adv. Funct. Mater.*, 2008, **18**, 2328.

16 D. Li and Y. Zhu, *CrystEngComm*, 2012, **14**, 1128.
17 F. Amano, A. Yamakata, K. Nogami, M. Osawa and B. Ohtani, *J. Am. Chem. Soc.*, 2008, **130**, 17650.
18 M. Shang, W. Wang and H. Xu, *Cryst. Growth Des.*, 2009, **9**, 991.
19 X. Zhao and Y. Zhu, *Environ. Sci. Technol.*, 2006, **40**, 3367.
20 H. Fu, L. Zhang, W. Yao and Y. Zhu, *Appl. Catal., B*, 2006, **66**, 100.
21 H. Fu, J. Lin, L. Zhang and Y. Zhu, *Appl. Catal., A*, 2006, **306**, 58.
22 G. Huang, C. Zhang and Y. Zhu, *J. Alloys Compd.*, 2007, **432**, 269.
23 J. Lin, J. Lin and Y. Zhu, *Inorg. Chem.*, 2007, **46**, 8372.
24 R. Shi, Y. Wang, D. Li, J. Xu and Y. Zhu, *Appl. Catal., B*, 2010, **100**, 173.
25 D. Li, R. Shi, C. Pan, Y. Zhu and H. Zhao, *CrystEngComm*, 2011, **13**, 4695.
26 D. Ye, D. Li, W. Zhang, M. Sun, Y. Hu, Y. Zhang and X. Fu, *J. Phys. Chem. C*, 2008, **112**, 17351.
27 W. Tong, L. Li, W. Hu, T. Yan and G. Li, *J. Phys. Chem. C*, 2010, **114**, 1512.
28 D. Li, X. Bai, J. Xu, X. Ma and Y. Zhu, *Phys. Chem. Chem. Phys.*, 2014, **16**, 212.
29 M. Niederberger and H. Cölfen, *Phys. Chem. Chem. Phys.*, 2006, **8**, 3271.
30 S. U. M. Khan, M. Al-Shahry and W. B. Ingler Jr., *Science*, 2002, **27**, 2243.
31 K. H. Ji, D. M. Jang, Y. J. Cho, Y. Myung, H. S. Kim, Y. Kim and J. Park, *J. Phys. Chem. C*, 2009, **113**, 19966.
32 L. Zhang, Y. Wang, H. Cheng, W. Yao and Y. Zhu, *Adv. Mater.*, 2009, **21**, 1286.
33 L. Zhang, H. Cheng, R. Zong and Y. Zhu, *J. Phys. Chem. C*, 2009, **113**, 2368.
34 S. Zhu, T. Xu, H. Fu, J. Zhao and Y. Zhu, *Environ. Sci. Technol.*, 2007, **41**, 6234.
35 K. Kabra, R. Chaudhary and R. L. Sawhney, *J. Hazard. Mater.*, 2008, **155**, 424.
36 H. Fu, C. Pan, W. Yao and Y. Zhu, *J. Phys. Chem. B*, 2005, **109**, 22432.
37 M. R. Hoffmann, S. T. Martin, W. Choi and D. W. Bahneman, *Chem. Rev.*, 1995, **95**, 69.
38 T. Mohammad and H. Morrison, *Photochem. Photobiol.*, 2000, **71**, 369.
39 T. Zhang, T. Oyama, A. Aoshima, H. Hidaka, J. Zhao and N. Serpone, *J. Photochem. Photobiol., A*, 2001, **140**, 163.
40 C. Pan, J. Xu, Y. Wang, D. Li and Y. Zhu, *Adv. Funct. Mater.*, 2012, **22**, 1518.
41 Y. Wang, Z. Wang, S. Muhammad and J. He, *CrystEngComm*, 2012, **14**, 5065.
42 I. Aslam, C. Cao, M. Tanveer, M. H. Faroog, W. S. Khan, M. Tahir, F. Idrees and S. Khalid, *RSC Adv.*, 2015, **5**, 6019.